ISSN 2218-4333 (online)

World Journal of *Clinical Oncology*

World J Clin Oncol 2024 March 24; 15(3): 360-463

Published by Baishideng Publishing Group Inc

World Journal of Clinical Oncology

Contents

Monthly Volume 15 Number 3 March 24, 2024

World Journal of Clinical Oncology

Monthly Volume 15 Number 3 March 24, 2024

Contents

World Journal of Clinical Oncology

Monthly Volume 15 Number 3 March 24, 2024

Contents

ABOUT COVER

Peer Reviewer of *World Journal of Clinical Oncology*, Alessandro Posa, MD, Department of Diagnostic Imaging, Oncologic Radiotherapy and Hematology, Fondazione Policlinico Universitario A. Gemelli - IRCCS, Rome 00168, RM, Italy. alessandro.posa@policlinicogemelli.it

AIMS AND SCOPE

The primary aim of *World Journal of Clinical Oncology* (*WJCO*, *World J Clin Oncol*) is to provide scholars and readers from various fields of oncology with a platform to publish high-quality basic and clinical research articles and communicate their research findings online.

WJCO mainly publishes articles reporting research results and findings obtained in the field of oncology and covering a wide range of topics including art of oncology, biology of neoplasia, breast cancer, cancer prevention and control, cancer-related complications, diagnosis in oncology, gastrointestinal cancer, genetic testing for cancer, gynecologic cancer, head and neck cancer, hematologic malignancy, lung cancer, melanoma, molecular oncology, neurooncology, palliative and supportive care, pediatric oncology, surgical oncology, translational oncology, and urologic oncology.

INDEXING/ABSTRACTING

The *WJCO* is now abstracted and indexed in PubMed, PubMed Central, Emerging Sources Citation Index (Web of Science), Reference Citation Analysis, China Science and Technology Journal Database, and Superstar Journals Database. The 2023 Edition of Journal Citation Reports® cites the 2022 impact factor (IF) for *WJCO* as 2.8; IF without journal self cites: 2.8; 5-year IF: 3.0; Journal Citation Indicator: 0.36.

RESPONSIBLE EDITORS FOR THIS ISSUE

NAME OF JOURNAL
World Journal of Clinical Oncology

ISSN
ISSN 2218-4333 (online)

LAUNCH DATE
November 10, 2010

FREQUENCY
Monthly

EDITORS-IN-CHIEF
Hiten RH Patel, Stephen Safe, Jian-Hua Mao, Ken H Young

EDITORIAL BOARD MEMBERS
https://www.wjgnet.com/2218-4333/editorialboard.htm

PUBLICATION DATE
March 24, 2024

INSTRUCTIONS TO AUTHORS
https://www.wjgnet.com/bpg/gerinfo/204

GUIDELINES FOR ETHICS DOCUMENTS
https://www.wjgnet.com/bpg/GerInfo/287

GUIDELINES FOR NON-NATIVE SPEAKERS OF ENGLISH
https://www.wjgnet.com/bpg/gerinfo/240

PUBLICATION ETHICS
https://www.wjgnet.com/bpg/GerInfo/288

PUBLICATION MISCONDUCT
https://www.wjgnet.com/bpg/gerinfo/208

ARTICLE PROCESSING CHARGE
https://www.wjgnet.com/bpg/gerinfo/242

STEPS FOR SUBMITTING MANUSCRIPTS
https://www.wjgnet.com/bpg/GerInfo/239

ONLINE SUBMISSION
https://www.f6publishing.com

World Journal of Clinical Oncology

Submit a Manuscript: https://www.f6publishing.com

World J Clin Oncol 2024 March 24; 15(3): 419-433

DOI: 10.5306/wjco.v15.i3.419

ISSN 2218-4333 (online)

ORIGINAL ARTICLE

Prospective Study

Nomogram based on multimodal magnetic resonance combined with B7-H3mRNA for preoperative lymph node prediction in esophagus cancer

Yan-Han Xu, Peng Lu, Ming-Cheng Gao, Rui Wang, Yang-Yang Li, Rong-Qi Guo, Wei-Song Zhang, Jian-Xiang Song

Specialty type: Oncology

Provenance and peer review: Unsolicited article; Externally peer reviewed.

Peer-review model: Single blind

Peer-review report's scientific quality classification

Grade A (Excellent): 0
Grade B (Very good): B
Grade C (Good): 0
Grade D (Fair): 0
Grade E (Poor): 0

P-Reviewer: Shiryajev YN, Russia

Received: November 19, 2023
Peer-review started: November 19, 2023
First decision: January 9, 2024
Revised: January 15, 2024
Accepted: February 6, 2024
Article in press: February 6, 2024
Published online: March 24, 2024

Yan-Han Xu, Ming-Cheng Gao, Rui Wang, Yang-Yang Li, Rong-Qi Guo, Wei-Song Zhang, School of Clinical Sciences, Graduate School of Nantong University, Yancheng 226019, Jiangsu Province, China

Yan-Han Xu, Ming-Cheng Gao, Rui Wang, Yang-Yang Li, Rong-Qi Guo, Wei-Song Zhang, Jian-Xiang Song, Department of Thoracic Surgery, Yancheng Third People's Hospital, The Affiliated Hospital 6 of Nantong University, Yancheng 224000, Jiangsu Province, China

Peng Lu, Department of Imaging, Yancheng Third People's Hospital, The Affiliated Hospital 6 of Nantong University, Yancheng 224000, Jiangsu Province, China

Corresponding author: Jian-Xiang Song, MD, PhD, Chief Doctor, Chief Physician, Dean, Doctor, Surgeon, Department of Thoracic Surgery, Yancheng Third People's Hospital, The Affiliated Hospital 6 of Nantong University, No. 2 Xindu West Road, Yandu Street, Yandu District, Yancheng 224000, Jiangsu Province, China. jxsongycsy@163.com

Abstract

BACKGROUND

Accurate preoperative prediction of lymph node metastasis (LNM) in esophageal cancer (EC) patients is of crucial clinical significance for treatment planning and prognosis.

AIM

To develop a clinical radiomics nomogram that can predict the preoperative lymph node (LN) status in EC patients.

METHODS

A total of 32 EC patients confirmed by clinical pathology (who underwent surgical treatment) were included. Real-time fluorescent quantitative reverse transcription-polymerase chain reaction was used to detect the expression of B7-H3 mRNA in EC tissue obtained during preoperative gastroscopy, and its correlation with LNM was analyzed. Radiomics features were extracted from multi-modal magnetic resonance imaging of EC using Pyradiomics in Python. Feature extraction, data dimensionality reduction, and feature selection were performed using XGBoost model and leave-one-out cross-validation. Mul-

tivariable logistic regression analysis was used to establish the prediction model, which included radiomics features, LN status from computed tomography (CT) reports, and B7-H3 mRNA expression, represented by a radiomics nomogram. Receiver operating characteristic area under the curve (AUC) and decision curve analysis (DCA) were used to evaluate the predictive performance and clinical application value of the model.

RESULTS

The relative expression of B7-H3 mRNA in EC patients with LNM was higher than in those without metastasis, and the difference was statistically significant ($P < 0.05$). The AUC value in the receiver operating characteristic (ROC) curve was 0.718 (95%CI: 0.528-0.907), with a sensitivity of 0.733 and specificity of 0.706, indicating good diagnostic performance. The individualized clinical prediction nomogram included radiomics features, LN status from CT reports, and B7-H3 mRNA expression. The ROC curve demonstrated good diagnostic value, with an AUC value of 0.765 (95%CI: 0.598-0.931), sensitivity of 0.800, and specificity of 0.706. DCA indicated the practical value of the radiomics nomogram in clinical practice.

CONCLUSION

This study developed a radiomics nomogram that includes radiomics features, LN status from CT reports, and B7-H3 mRNA expression, enabling convenient preoperative individualized prediction of LNM in EC patients.

Key Words: Esophageal cancer; Radiomics; B7-H3mRNA; Multimodal magnetic resonance imaging; Lymph node metastasis; Nomogram

Core Tip: Accurate tumor-node-metastasis staging plays a critical role in devising treatment strategies for esophageal cancer (EC), particularly in assessing lymph node (LN) metastasis. Nevertheless, existing techniques for diagnosing LN in EC are currently constrained by limited accuracy. In light of this, our study endeavors to construct a clinical column chart that can enhance the assessment of LN status, furnishing a valuable point of reference for the diagnosis and treatment of EC.

Citation: Xu YH, Lu P, Gao MC, Wang R, Li YY, Guo RQ, Zhang WS, Song JX. Nomogram based on multimodal magnetic resonance combined with B7-H3mRNA for preoperative lymph node prediction in esophagus cancer. *World J Clin Oncol* 2024; 15(3): 419-433

URL: https://www.wjgnet.com/2218-4333/full/v15/i3/419.htm

DOI: https://dx.doi.org/10.5306/wjco.v15.i3.419

INTRODUCTION

According to relevant research statistics, esophageal cancer (EC) is a common malignant tumor in the field of thoracic surgery, ranking seventh in terms of incidence and sixth in terms of mortality worldwide. In Asia, the main histological type is squamous cell carcinoma[1-3]. Most EC patients require comprehensive treatment. In the early stage, surgery or endoscopic resection is the primary approach, while concurrent chemoradiotherapy is preferred for patients in the middle and late stages. The specific treatment plan should be based on the accurate staging of EC using the tumor-node-metastasis (TNM) classification system[4].

Simultaneously, in surgical treatment, due to the highly variable lymphatic spread of cancer, suspicious positive lymph nodes (LN) should be resected together with the tumor to improve patient survival. However, some studies suggest that expanding the range of LN dissection may increase postoperative complications and worsen prognosis for cancer patients [5,6]. Therefore, in the formulation of treatment strategies for EC, accurate diagnosis of LN metastasis (LNM) status is crucial[7,8].

B7-H3, also known as CD276, is a member of the B7 Ligand family and is an attractive target in antibody immunotherapy. It is overexpressed on many malignant cells and cancer stem cells but exhibits low-level expression in normal tissues[9]. Relevant studies have shown that B7-H3 primarily promotes tumor development through immune mechanisms by inhibiting specific immune responses, leading to a pro-tumoral effect[9]. Research has found associations between B7-H3 expression and clinical TNM progression and prognosis in diseases such as gastric cancer, pancreatic cancer, colorectal cancer, lung cancer, and acute myeloid leukemia[10-15]. Additionally, Arigami *et al*[16] discovered a strong correlation between B7-H3 expression and sentinel LNM and the number of LNM in their study of breast cancer. In their multivariate analysis, the mRNA expression of B7-H3 in the primary tumor significantly predicted regional LNM [16]. Furthermore, Chen *et al*[17] found a close association between B7-H3 expression in EC and aggressive biology, low tumor-infiltrating T lymphocyte density, and poor prognosis[17]. However, there is currently no relevant research proving an association between B7-H3 expression and LNM in EC.

Currently, computed tomography (CT) is commonly used to determine the preoperative LN status in EC patients, primarily relying on size-based measurements (*e.g.*, a 10 mm short-axis diameter on CT as the cutoff value for diagnosing LNM)[18]. However, relevant studies have shown that this method has an accuracy rate of less than 70% in determining LNM[19]. Positron emission tomography (PET)/CT is a rapidly developing imaging modality that combines positron emission tomography with X-ray CT. However, its application in LNM diagnosis is limited due to its high cost, low sensitivity, and high false-positive rate[20]. Meanwhile, research on positive LN detection in certain cancers suggests that magnetic resonance imaging (MRI) has higher accuracy[21,22]. However, conventional MRI of the chest is prone to motion artifacts due to respiratory motion, which can affect image quality. With the emergence of multi-sequence MRI techniques such as StarVIBE and T2TSE-BLADE, respiratory motion artifacts in non-breath-hold patients and uncooperative patients have been significantly reduced, resulting in clearer visualization of tumors and the surrounding soft tissue boundaries and improved image quality[23,24]. However, existing imaging modalities primarily rely on LN anatomy, and their assessment of LNM is based on size measurements, which are insufficient to reveal the internal structural characteristics of LN and obtain valuable tumor-related information[25].

Radiomics research involves applying computer mathematical tools to image processing, extracting radiological features such as shape, texture, or waveform, which can provide information about cancer phenotypes and the tumor microenvironment. This concept was introduced by Lambin *et al*[26] in 2012. By combining radiomics-derived data with other relevant data, accurate and reliable Clinical Decision Support Systems (CDSS) can be generated[27]. Currently, radiomics has made significant progress in the qualitative assessment of tumors, diagnosis of LNM, and prognosis prediction[28-30]. However, there is currently no research that combines radiomics with expression factors in primary tumors to elucidate their diagnostic and predictive value in cancer. This integration could contribute to a more comprehensive understanding of the biological characteristics and behavior of tumors, providing more accurate predictions for individualized treatment.

Therefore, the objective of this study is to develop a radiomics nomogram that combines radiomic features, B7-H3 mRNA expression levels, and clinical risk factors for individualized prediction of preoperative LNM in EC patients.

MATERIALS AND METHODS

Patients

Our research institution's ethics review committee (the Medical Ethics Committee of the Sixth Affiliated Hospital of Nantong University, Yancheng Third People's Hospital) has approved this research project. Considering that the relevant examinations in this study do not pose significant physical or harm to the patients' interests, the requirement for obtaining informed consent from the patients has been waived by the committee. Our study included a total of 32 EC patients (9 females and 23 males) who received treatment at our hospital from March 2022 to July 2023 and met the inclusion criteria of this study. The patients had an average age of 70.53 ± 6.41 years, with an age range of 52-84 years. The inclusion criteria were as follows: (1) All patients were over 18 years of age; (2) Standard contrast-enhanced CT and MRI examinations were performed within 10 d before treatment; (3) Patients underwent gastroscopy and pathological biopsy at our hospital, and the pathological diagnosis was confirmed as esophageal squamous cell carcinoma; (4) The surgical approach was consistent for all patients, with three-field LN dissection for EC; (5) MRI images had sufficient clarity to support radiomic feature extraction; (6) Availability of clinical and pathological information; and (7) B7-H3 mRNA expression was determined by reverse transcription-polymerase chain reaction (RT-PCR) using cancer tissue samples obtained from preoperative esophagoscopic biopsies. The exclusion criteria were as follows: (1) Patients with significant surgical contraindications; (2) Patients with concurrent other tumor diseases; and (3) Inability to undergo MRI examination or presence of contraindications for MRI examination. The patients recruitment and selection process was showed in Figure 1.

Baseline clinical information and pathological data of the patients in the study, including age, sex, tumor location, tumor size, and LN status (based on pathological results), were obtained from medical records. In addition, the enhanced CT reports of the study patients were collected, and LN with a size of ≥ 10.0 mm in the CT reports were considered as positive for LN involvement.

Image acquisition and segmentation

The patients were scanned using a 3.0T MRI scanner (MAGNETOM Skyra 3.0T, Siemens Healthcare, Germany) and an 18-channel surface phased-array coil. Prior to the examination, patients were instructed to remove any metallic objects and undergo respiratory training. The patients were positioned in a supine position with the head first, and the scanning range extended from the bilateral lung apices to 1 cm below the diaphragm. The MRI scanning sequences included T1-Star-VIBE and T2-TSE-BLADE sequences. The parameters for the T1-Star-VIBE sequence were as follows: TR/TE = 3.98/1.91 ms; voxel size = 1.0 mm × 1.0 mm × 1.0 mm; FOV = 300 mm × 300 mm; flip angle = 12°; scanning time = 309 s. The parameters for the T2-TSE-BLADE sequence were as follows: TR/TE = 5000/97 ms; voxel size = 0.9 mm × 0.9 mm × 3.0 mm; FOV = 260 mm × 260 mm; flip angle = 180°; scanning time = 360-600 s.

We retrieved the MRI images of all patients from the hospital's Picture Archiving and Communication System. Preprocessing of the acquired images was performed using Python, which included bias field correction utilizing the N4 correction algorithm and registration alignment. Subsequently, image feature segmentation and analysis were conducted. These processes aimed to extract meaningful features from the images, facilitating further analysis and the development of our study's models.

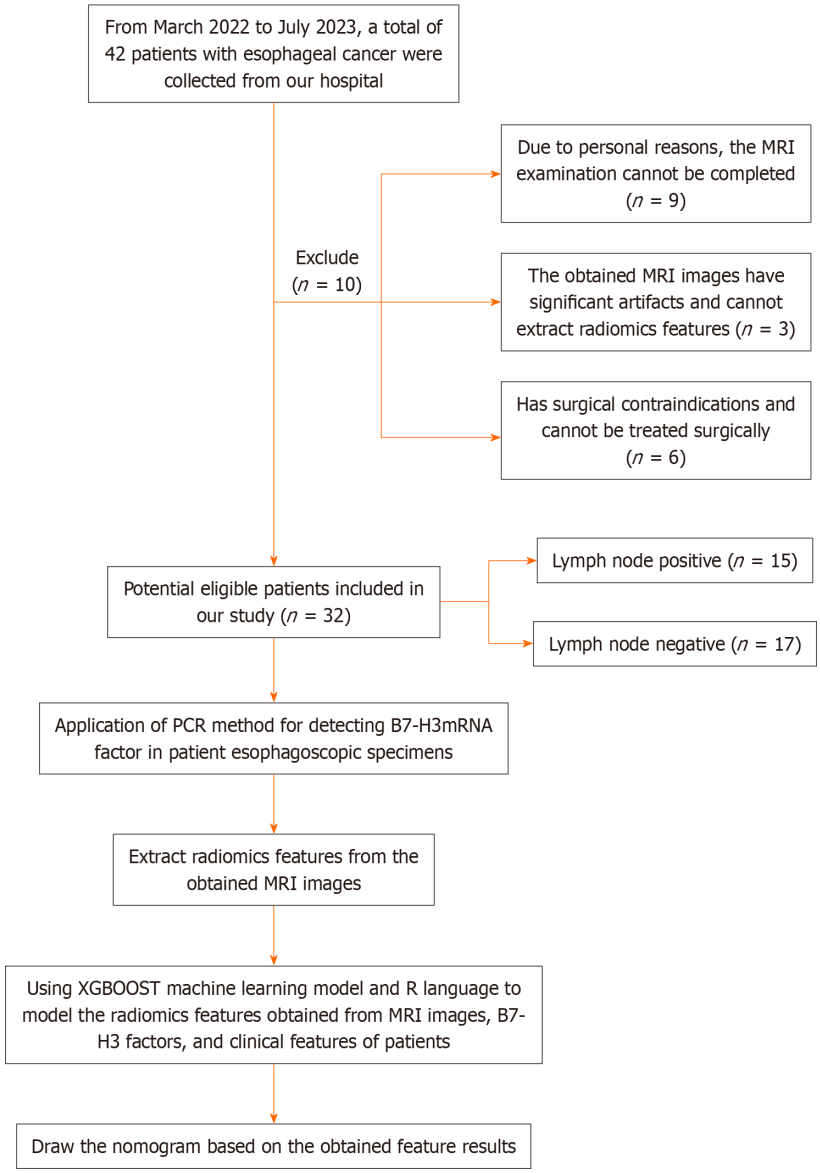

Figure 1 Recruitment and selection process of patients. MRI: Magnetic resonance imaging; PCR: Polymerase chain reaction.

The three-dimensional (3D) semi-automatic segmentation was performed by a single operator, who was a thoracic surgery graduate student, using the 3D Slicer software. The segmentation process involved the extraction of valuable regions of interest (ROIs) based on the radiologist's interpretation. The radiologist, with 10 years of experience in the field, provided the expert assessment of the images, and the operator utilized this information to guide the segmentation and extraction of the ROIs. The operator carefully followed the radiologist's findings to ensure accurate and reliable segmentation of the desired regions.

In this study, ROIs referred to the primary lesions of EC. These ROIs were manually delineated on each consecutive slice of the MRI images along the boundaries of the primary tumor lesions. The delineation process excluded adjacent air, blood vessels, fat, and normal tissues, focusing solely on the pathological features of the primary tumor. The delineation was performed by the operator using the 3D Slicer software, guided by the radiologist's interpretation and expertise.

Radiomics feature extraction and selection

We applied the PyRadiomics component in Python (https://pyradiomics.readthedocs.io/en/Latest/) to extract features from the ROI for each case. Prior to ROI processing, we performed bias field correction (N4 correction) and registration alignment on every MRI image of all sequences to mitigate the impact of varying grayscale ranges in PyRadiomics. The extracted feature categories include first-order, shape, gray level co-occurrence matrix, gray level run length matrix, gray level size zone matrix, gray level dependence matrix, and neighboring gray tone difference matrix.

Due to the limited sample size in this study, we employed the XGBoost model and leave-one-out cross-validation method to construct the radiomics features. Firstly, a *t*-test was applied to select the top 30% features that are predictive of LNM. Secondly, using the leave-one-out cross-validation method, internal cross-validation was performed to further retain features that improve diagnostic performance. Finally, the radiomics signature and its corresponding weight values were computed to obtain the consistency features in the model. The specific formula for the established and

extracted radiomics features is as follows:

Radiomics signature = Intercept + coef 1 × feature 1 + coef 2 × feature 2 + coef 3 × feature 3 + coef 4 × feature 4 + coef 5 × feature 5 + ... + coef *n* × feature *n*.

Real-time quantitative RT-PCR

Acquisition of esophageal pathological tissue under esophagoscopy: Patients diagnosed with EC were carefully screened for inclusion in the study. Under gastroscopy, specialized endoscopic forceps were used to obtain biopsy specimens from suspected cancerous lesions. Additionally, samples of normal tissue were collected from a location at least 5 cm away from the suspected cancerous area to serve as adjacent normal tissue. Following the collection of cancerous and adjacent normal tissue, the specimens were immediately immersed and washed in physiological saline solution. Subsequently, they were stored at a temperature of -80 °C in a freezer for preservation. To ensure the accuracy and reliability of the study, specimens that did not meet the predefined inclusion criteria were carefully excluded. This exclusion process was based on a combination of subsequent patient treatment and pathological diagnosis, which served as the gold standard.

RNA extraction from specimen tissue: (1) Tissue lysis: The collected specimens of EC and adjacent normal tissue were removed from the -80 °C freezer and thawed. On a sterile bench, the tissue was finely minced using sterile tissue scissors. Approximately 0.2 g of the tissue was weighed on an electronic precision balance and transferred into a grinding tube. The tissue was then washed with PBS buffer (dissolving protective reagent) for 5 min. The grinding tube containing the tissue was placed on ice.

Next, 500 μL of RNA extraction solution (*e.g.*, RNA Extrizol) was added to the grinding tube using a pipette. A handheld tissue grinder was used, adjusting it to the maximum speed, to grind the tissue in a start-stop manner. Care was taken to avoid liquid splashing during the grinding process. Grinding was continued until the tissue was completely lysed and formed a homogenized liquid. Finally, 500 μL of RNA extraction solution was added and mixed well with the lysate.

Subsequently, 200 μL of chloroform solvent (trichloromethane) was added to the tube. The tube was then placed on a shaker and shaken for 15 s. After shaking, the tube was left to stand at room temperature for 3 min.

(2) RNA Precipitation and Washing: The pre-cooled centrifuge was set to a temperature of 4 °C. The centrifuge speed was adjusted to 13000 rpm, and the centrifugation time was set to 15 min. The tubes containing the lysed tissue were placed in the centrifuge and balanced before initiating centrifugation. After 15 min of centrifugation, the top layer of liquid (approximately 400 μL) from the tube was carefully extracted using a pipette and transferred to a new tube. It is important to only aspirate the top layer of liquid, avoiding any other layered liquids to prevent contamination of chromosomal DNA.

Using a pipette, 500 μL of isopropanol was added to the tube containing the extracted liquid, and the mixture was thoroughly mixed. The tube was then left to stand at room temperature for 10 min to allow RNA precipitation.

The centrifuge process was repeated as described above (centrifuge temperature set at 4 °C, centrifuge speed at 13000 rpm, and centrifugation time of 15 min). The tube was placed in the centrifuge and balanced before initiating centrifugation. After 15 min of centrifugation, a white, flocculent precipitate could be observed at the bottom of the centrifuge tube, which represented the RNA after lysis completion. Using a pipette, the entire supernatant, excluding the flocculent precipitate, was aspirated and discarded, while retaining the RNA pellet.

To wash the RNA pellet, 1 mL of 75% ethanol solvent was added to the centrifuge tube and mixed thoroughly. The centrifuge parameters were set to a temperature of 4 °C, a speed of 750 g, and a centrifugation time of 5 min. The tube was placed in the centrifuge, balanced, and then centrifuged.

And (3) RNA resuspension and concentration measurement: Using a pipette, carefully aspirate the upper ethanol solution from the centrifuge tube, being cautious not to draw up the white precipitate at the bottom. After aspirating the ethanol solution, let the centrifuge tube air dry at room temperature. Then, add 20 μL of nuclease-free water to the dried centrifuge tube to fully dissolve the RNA.

Next, measure the concentration and purity of the RNA in the centrifuge tube using a NANODROP 2000 nucleic acid and protein analyzer. Ensure that the absorbance ratio at 260 nm and 280 nm falls within the range of 1.8-2.0 for the retained samples to ensure accuracy of the measurement results. If the ratio falls outside this range, discard the sample and repeat the experiment with a new tissue specimen. Label the centrifuge tube containing the remaining RNA and store it in a -80 °C freezer for future experiments.

mRNA real-time quantitative polymerase chain reaction experimental steps: (1) cDNA synthesis by reverse transcription: RNA extraction solution was retrieved from a -80 °C freezer and transferred to a new microcentrifuge tube. Using a pipette, 3 μg of RNA was extracted as a template and mixed with 1 μL of Oligo (dT) primer solution. Then, nuclease-free water was added to achieve a total volume of 12 μL, and the mixture was gently mixed. The mixture was centrifuged for 10 s in a microcentrifuge.

Prior to the next step, a constant temperature incubator was pre-set at 70 °C for 5 min. The microcentrifuge tube containing the mixture was heated in the incubator. After heating, the tube was immediately transferred to an icebox for cooling, followed by a brief centrifugation to collect the precipitate.

Next, the reaction mixture was prepared. Using a pipette, 4 μL of 5 × Reaction Buffer, 1 μL of RNase Inhibitor, 2 μL of 10 mmol/L dNTP Mix, and 1 μL of RevertAid M-MuLV RT were drawn. Each microcentrifuge tube was then added with 8 μL of the reaction mixture, gently mixed, and centrifuged for 5 s in a microcentrifuge.

Prior to performing the reverse transcription reaction, the polymerase chain reaction (PCR) machine was pre-set to a temperature of 42 °C, and a 6 min wait was observed. Subsequently, the reaction was incubated at 72 °C for 5 min to

terminate the reverse transcription. The microcentrifuge tubes were placed in ice, and a 1:10 dilution was performed for storage at -20 °C.

And (2) Real-time quantitative PCR amplification and analysis: Retrieve an equal volume of cDNA template from the -20 °C freezer and place it in an EP tube. Add the amplification primers to achieve a total volume of 20 μL. Transfer the mixture to the PCR machine for further reaction.

Data analysis was performed using the 2-ΔCT relative quantification method, with β-actin as the reference gene for normalization. Each group included two technical replicates, and the procedure was as follows: Retrieve the standard EP tube and sequentially add 2 μL of template, 1 μL of upstream primer (concentration of 10 μmol/L), 1 μL of downstream primer (concentration of 10 μmol/L), 12.5 μL of SYBR Green Master Mix, and 8.5 μL of double distilled water. Gently mix the solution and centrifuge for 10 s in a microcentrifuge.

Perform amplification using the PCR machine. Each group contains three samples, and the program is set as follows: Pre-denaturation at 95 °C for 10 min, followed by 40 cycles of denaturation at 95 °C for 30 s, annealing at 60 °C for 30 s, and extension at 72 °C for 40 s. Finally, terminate the reaction at 72 °C for 10 min.

After the completion of the PCR amplification, data analysis was performed based on the amplification curve and melt curve. The 2-ΔΔCt relative quantification method was used for data analysis in each group, with β-actin as the internal reference gene for normalization. Each group included four samples, and three experimental replicates were performed. The final data analysis was conducted using GraphPad Prism 5.0 software.

Model construction

We utilized the R software to perform logistic regression analysis to identify independent predictive factors, including radiomic features, B7-H3 mRNA expression level, and LN status reported by CT, in our study. A model incorporating these independent predictors was developed, and its performance was evaluated using the area under the receiver operating characteristic (ROC) curve.

Nomogram development and decision curve analysis

Nomogram development and decision curve analysis (DCA) were employed for model visualization and clinical application. To assess the additional value of radiomic features, B7-H3 mRNA, and CT in individually predicting the preoperative LN status in EC patients, four decision curves were developed based on CT reports, radiomic features of the primary lesion, B7-H3 mRNA, and a combined model (including CT reports, B7-H3 mRNA, and radiomic features). These decision curves were used to further determine the clinical utility of the plotted line chart.

RESULTS

Clinical characteristics

The study included a total of 32 EC patients, as shown in Table 1. There were no significant differences ($P > 0.05$) between the LN-positive and LN-negative groups in terms of patient age, sex, preoperative carcinoembryonic antigen (CEA) levels, preoperative squamous cell carcinoma antigen levels, pathological grade, tumor location, and tumor size. However, a statistically significant difference was observed in T stage ($P < 0.05$). In the study cohort, the LNM rate was 46.88% (15/32) based on postoperative pathological diagnosis. Regarding the subjective enhanced CT reports of LN status, 6 patients were reported as LN-negative but confirmed to have LNM, while 6 patients were reported as LN-positive but confirmed to be LN-negative. The sensitivity was 60.0%, and the specificity was 64.7% (Table 1).

The relationship between the expression level of B7-H3 mRNA and the clinical characteristics of EC patients

The correlation between B7-H3 mRNA expression levels and age, sex, T stage, and N stage (LNM) in patients with EC was analyzed separately. The T stage and N stage of EC were determined according to the International 8th edition TNM staging criteria for EC.

Among the 32 patients with EC, the average B7-H3 mRNA expression level in male patients was 2.47 ± 0.51, while in female patients, it was 2.52 ± 0.40. There was no significant statistical difference between the two groups ($P > 0.05$). The results indicate that there is no significant correlation between B7-H3 mRNA expression levels and sex in patients with EC ($P > 0.05$).

Among the 32 patients with EC, the average B7-H3 mRNA expression level in T1 stage patients was 2.23 ± 0.32, in T2 stage patients it was 2.66 ± 0.53, and in T3 stage patients it was 2.59 ± 0.12. There was a significant correlation in the average B7-H3 mRNA expression levels among the different T stages ($P < 0.05$). Furthermore, we found that the average B7-H3 mRNA expression level in the tissues of EC patients with LNM was 2.70 ± 0.53, while in patients without LNM, it was 2.29 ± 0.35. The study revealed a significant increase in B7-H3 mRNA expression levels in the tissues of EC patients with LNM compared to those without LNM ($P < 0.05$; Figure 2A).

In conclusion, the expression level of B7-H3 mRNA in EC is not significantly correlated with sex ($P > 0.05$). However, it is closely associated with T stage and LNM in EC ($P < 0.05$). The relative expression level of B7-H3 mRNA is significantly higher in LN-positive tissues of esophageal squamous cell carcinoma, indicating an upregulation of B7-H3 mRNA expression in LN-positive tissues of EC (Table 2).

Diagnostic value of B7-H3 mRNA in detecting LNM in EC

We performed quantitative analysis of B7-H3 mRNA expression in 32 EC tissues and generated a ROC curve (Figure 1) to

Table 1 Characteristics of patients in the cohort, *n* (%)

Characteristic	LN metastasis (+)	LN metastasis (-)	*P* value
Age, mean ± SD	70.18 ± 6.75	71.92 ± 7.49	0.39
Tumor size, mean ± SD	3.89 ± 1.55	3.18 ± 1.64	0.24
Sex			0.54
Male	10 (66.67)	13 (76.47)	
Female	5 (33.33)	4 (23.53)	
CEA			0.99
0-5 ng/mL	15 (99.99)	16 (94.12)	
> 5 ng/mL	0 (0.01)	1 (5.88)	
Squamous cell carcinoma antigen			0.61
0-2.7 ng/mL	12 (80.0)	14 (82.35)	
> 2.7 ng/mL	3 (20.00)	3 (17.65)	
Location			0.99
Upper mediastinal	2 (13.33)	1 (5.88)	
Middle mediastinal	6 (40.00)	8 (47.06)	
Lower mediastinal	6 (40.00)	8 (47.06)	
Abdominal	1 (6.67)	0 (0.01)	
Histologic grade			0.40
Well differentiated	0 (0.01)	2 (11.77)	
Moderately differentiated	11 (73.33)	11 (64.71)	
Poorly differentiated	4 (26.67)	4 (23.53)	
T stage			0.01
1	3 (20.00)	10 (58.82)	
2	12 (80.00)	5 (29.41)	
3	0 (0.01)	2 (11.77)	
CT-reported LN status			0.16
0-10.0 mm	6 (40.00)	11 (64.71)	
> 10.0 mm	9 (60.00)	6 (35.29)	

LN: Lymph node; T: Tumor; CEA: Carcinoembryonic antigen; CT: Computed tomography.

evaluate the diagnostic value of B7-H3 in detecting LNM in EC using clinical pathological examination as the gold standard. The area under ROC curve (AUC) for B7-H3 in detecting LNM was 0.718, with a sensitivity of 73.3% and specificity of 70.6%. The optimal diagnostic threshold for B7-H3 in identifying LNM in EC was determined to be 2.56 (Figure 2A).

Feature extraction and model construction

Using the Pyradiomics package in Python, a total of 1169 radiomic features were extracted from MRI images. The feature selection process was performed using the Leave-one-out method from the XGBoost model, resulting in the reduction of the feature set to 18 potential predictive factors (Figure 3). In the LASSO regression model, the following features were identified as having non-zero coefficients:

T1-log-sigma-2-0-mm-3D_glcm_DifferenceAverage, T1-log-sigma-5-0-mm-3D_glszm_SizeZoneNonUniformityNormalized, T1-wavelet-LLH_gldm_LargeDependenceEmphasis, T1-wavelet-LHL_firstorder_Median, T1-wavelet-LHL_firstorder_RootMeanSquared, T1-wavelet-LHH_glcm_Contrast, T1-wavelet-LHH_glcm_JointEntropy, T1-wavelet-LHH_glszm_SmallAreaHighGrayLevelEmphasis, T1-wavelet-HLH_firstorder_MeanAbsoluteDeviation, T1-wavelet-HLH_glszm_SmallAreaEmphasis, T1-wavelet-HLH_glszm_SmallAreaHighGrayLevelEmphasis, T1-wavelet-HHL_glcm_ClusterTendency, T1-wavelet-HHL_glcm_Contrast, T1-wavelet-HHL_glszm_GrayLevelNonUniformity, T1-wavelet-HHH_firstorder_InterquartileRange, T2-original_gldm_DependenceEntropy, T2-log-sigma-4-0-mm-3D_glszm_GrayLevelNonUniformity, T2-wavelet-HLH_glcm_Idn. Additionally, the optimal weight value feature was

Table 2 The relationship between B7-H3 expression and clinical characteristics of esophageal cancer patients

Clinical characteristic	Number of sample	B7-H3mRNA	Statistic	*P* value
Sex				
Male	23	2.47 ± 0.51	0.06	0.80
Female	9	2.52 ± 0.40		
T			*F* statistic	
1	13	2.23 ± 0.32	3.309	0.05
2	17	2.66 ± 0.53		
3	2	2.59 ± 0.12		
N				
0	17	2.29 ± 0.35	2.50	0.02
1-3	15	2.70 ± 0.53		

T: Tumor; N: Node.

Table 3 Values of various coefficients in the nomogram

Variables	Coef	95%CI
T1.WM	-0.5717	(-2.85, -0.25)
T1-wavelet-LHL_firstorder_Median		
T1.W.HSAHGE	0.22695	(-0.21, -2.91)
HLH_glszm_SmallAreaHighGrayLevelEmphasis		
T1.W.CT	-2.1616	(-3.72, -0.87)
T1-wavelet-HHL_gicm_ClusterTendency		
T1.W.R	0.49155	(-1.02, -3.32)
T1-wavelet		
HHH_firstorder_InterquartileRange	-4.1807	(-4.97, -0.68)
T2.O.DE		
T2-original_gldm_DependenceEntropy	47.4461	(-0.67, -3.38)
T2.W.gl		
T2-wavelet-HLH_gicm_Idn	3.69379	(0.18, -4.34)
B7.H3		
CT	1.46262	(-1.98, -4.90)

The coefficient values of individual independent factors in the developed column chart are shown in the figure. The selected radiomic features and their abbreviations in the nomogram are presented in the table. All predictive factors have a *P* value < 0.05, indicating statistical significance. CT: Computed tomography.

determined to be T1-wavelet-HLH_glcm_InverseVariance through further calculations and analysis.

Subsequently, logistic regression analysis was conducted in R language to further determine the independent predictive factors among the selected radiomic features, B7-H3 mRNA expression level, T stage, and LN status from CT reports. During the analysis, the model with the smallest Akaike information criterion (AIC) value was chosen.

The following radiomic features were further selected:

T1-wavelet-LHL_firstorder_Median, T1-wavelet-HLH_glszm_SmallAreaHighGrayLevelEmphasis, T1-wavelet-HHL_glcm_ClusterTendency, T1-wavelet-HHH_firstorder_InterquartileRange, T2-original_gldm_DependenceEntropy, T2-wavelet-HLH_glcm_Idn (the corresponding coefficient values for each independent predictive factor are detailed in Table 3).

A model incorporating these independent predictive factors was developed and presented in the form of a column chart (Figure 4).

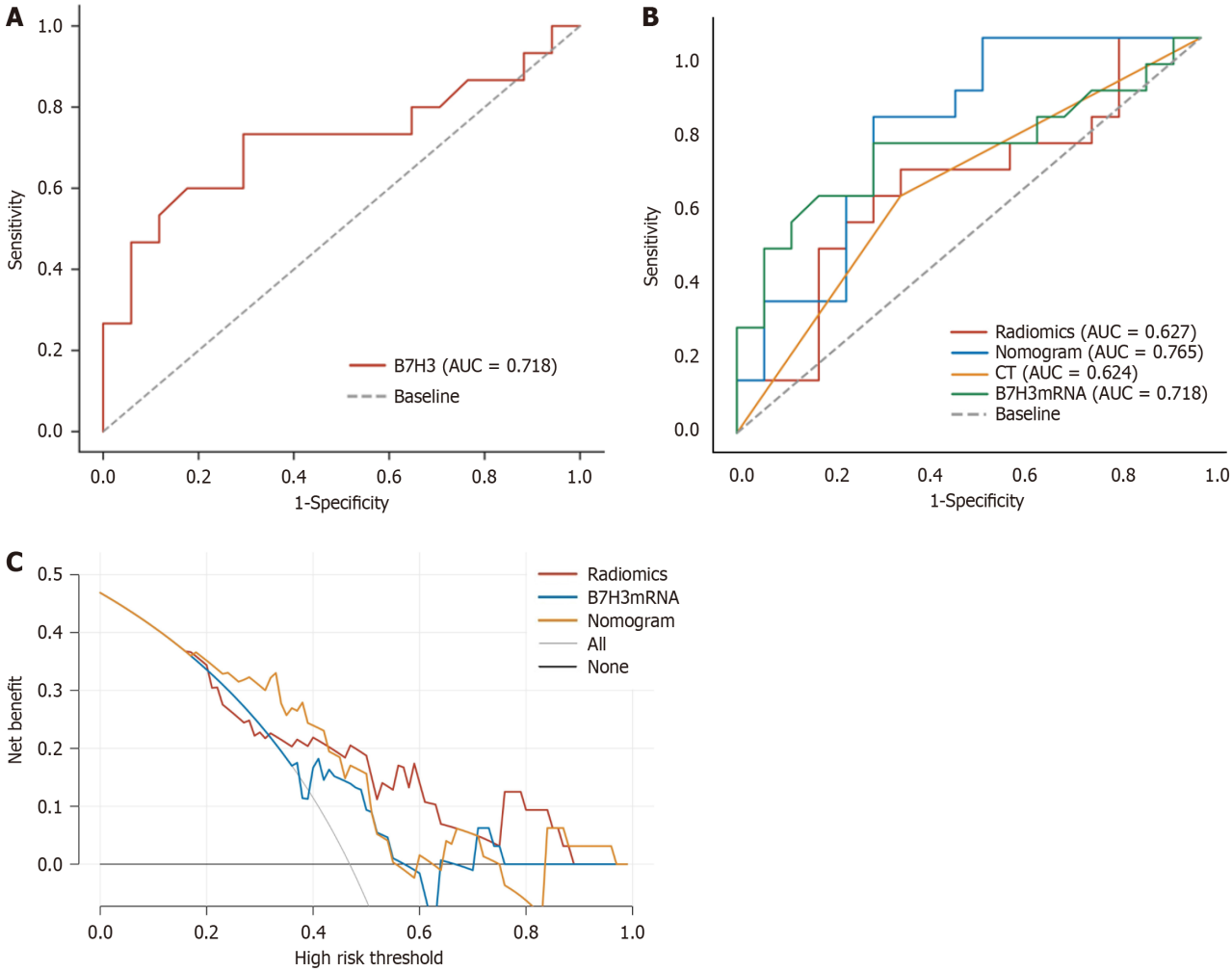

Figure 2 Receiver operating characteristic curve, the area under the receiver operating characteristic curve, and decision curve analysis. A: Receiver operating characteristic (ROC) curve of B7-H3mRNA in the study queue; B: Model performance in the study cohort. the area under the ROC curve (AUC) value increases when radiomic features are combined with B7-H3 mRNA expression compared to different feature combinations. Additionally, it can be observed that as more feature species are used, the AUC value increases, indicating better model performance; C: Decision curve analysis. The y-axis represents net benefit. The threshold probability refers to the point at which the perceived benefit of treating patients with intermediate to high-risk lymph node metastasis is considered equivalent to the harm of overtreating low-risk disease, reflecting how patients weigh the benefits and harms associated with decision-making. The higher curve at any given threshold probability represents the optimal prediction that maximizes net benefit. The decision curve indicates that the combined predictive model used provides greater net benefit compared to other models. AUC: The area under the receiver operating characteristic curve; CT: Computed tomography.

Clinical use

Using the pathological examination results as the gold standard, we calculated the diagnostic sensitivity and specificity of LN status from CT reports, B7-H3 mRNA expression, MRI radiomic features, and the combined predictive model for LNM in EC. The results are shown in Table 4. Furthermore, we plotted ROC curves (Figure 4) to illustrate the diagnostic performance of LN status from CT reports, B7-H3 mRNA expression, MRI radiomic features, and the established combined predictive model for preoperative LN diagnosis. Through comparison, we found that the combined predictive model exhibited the best discriminative power and predictive stability, with the highest AUC value (Table 4, Figure 1B).

The DCA based on combined predictive model is presented in Figure 1C. Compared to DCA using a single radiomic feature, the combined predictive model incorporating B7-H3 mRNA expression and clinical CT results demonstrates higher accuracy in predicting preoperative LN status. This indicates that the nomogram based on this predictive model is a reliable clinical tool for predicting LN status in patients with EC. The DCA suggests that within the probability threshold range of approximately 0.3 to 0.7, the nomogram based on the combined model provides additional net benefit to the "treatment" strategy.

DISCUSSION

LN status is one of the most important prognostic factors in EC, especially the number and location of metastatic LN, which are closely linked to clinical treatment decisions, including the implementation of neoadjuvant therapy, the extent of surgical LN resection, or the design of radiation therapy fields[25,31,32]. The decision of whether neoadjuvant

Table 4 Receiver operating characteristic curve of the dataset

Model	AUC (95%CI)	Sensitivity	Specificity	Youden index
Radiomics	0.627 (0.427-0.828)	0.667	0.647	0.314
Nomogram	0.765 (0.598-0.931)	0.800	0.706	0.506
CT	0.624 (0.426-0.821)	0.600	0.647	0.247
B7-H3mRNA	0.718 (0.528-0.907)	0.733	0.706	0.439

CT: Computed tomography; AUC: Area under the curve.

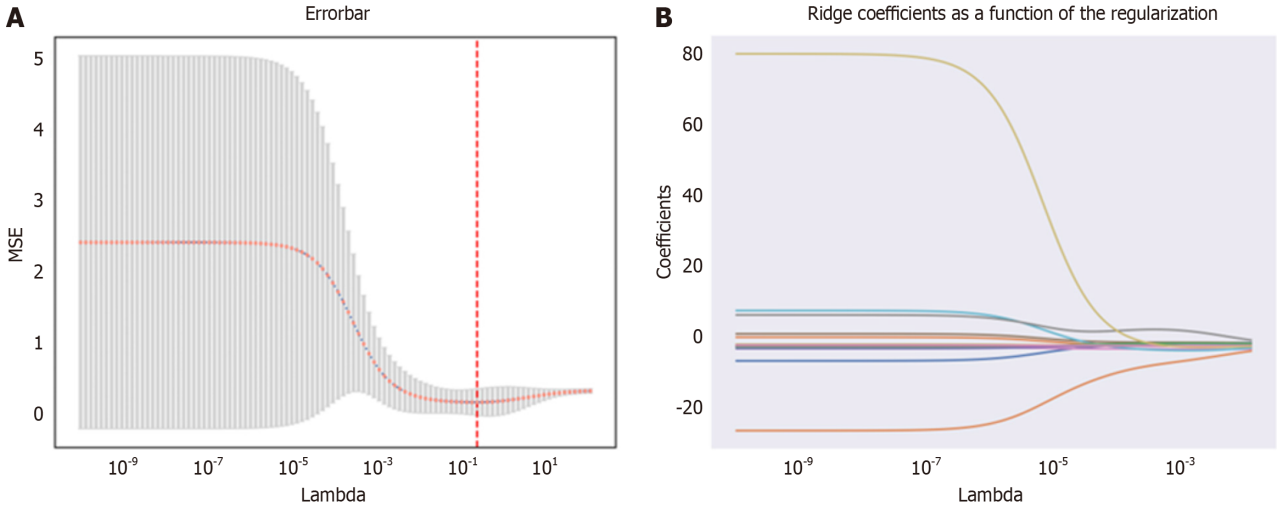

Figure 3 Texture feature selection using the Least Absolute Shrinkage and Selection Operator binary logistic regression model. A: The tuning parameter (Lambda) selection in the Least Absolute Shrinkage and Selection Operator (LASSO) model was performed using 10-fold cross-validation with the minimum criterion. The relationship curve between the mean-square error and Lambda is depicted, with a dashed line indicating the optimal value. The vertical lines represent the values selected through 10-fold cross-validation, including 18 optimized non-zero coefficients; B: LASSO coefficient profiles of 1169 texture features. The coefficient profiles were generated based on the sequence of log (Lambda). When using the value selected by 10-fold cross-validation, the optimal Lambda resulted in 18 non-zero coefficients. MSE: Mean-square error.

chemoradiotherapy is required before surgery primarily depends on the LN status. Furthermore, neoadjuvant chemoradiotherapy can target micrometastases, including LN metastases, and patients with LNM may benefit from this treatment [7,33]. However, for patients who refuse or are unable to tolerate surgery, the LN status cannot be diagnosed through postoperative biopsy. Therefore, accurate preoperative prediction of LN status is necessary and important.

With the advancement of radiomics research, an increasing number of studies are utilizing radiological features extracted from medical images, such as shape, texture, or waveform, to obtain a range of information about cancer phenotypes and the tumor microenvironment[27]. This information is distinct and complementary to other relevant data, including clinical features, treatment-related decision information, or genomic data[34]. When radiomics-derived data is combined with other relevant data and correlated with clinical disease outcomes, they can generate accurate and reliable CDSS[35,36]. These CDSS can assist clinicians in making more informed decisions regarding the diagnosis, treatment planning, and prognosis of cancer patients.

Unlike many previous studies on radiological features, which focused solely on the association of clinical and radiological features with tumor microenvironment characteristics in LNM, they neglected the impact of various proteins or tumor factors on promoting LNM[37-42]. In the study by Toiyama *et al*[43], they observed improved predictive accuracy when adding serum biomarkers to the predictive model as clinical pathological risk factors for preoperative detection of LNM in colorectal cancer patients [the area under the curve increased to 0.801 (95%CI: 0.725-0.857) with modification of the multivariate model]. Similarly, Huang *et al*[29] provided a radiomics nomogram incorporating radiomic features, LN status from CT reports, and CEA levels, which demonstrated higher accuracy in the preoperative individualized prediction of LNM in colorectal cancer patients. These studies may support the notion that considering tumor diagnostic biomarkers across different aspects is an important research approach to enhance CDSS[44].

In our previous studies, we demonstrated a close association between high expression of B7-H3 and tumor differentiation, TNM staging, and LNM in EC. In this study, we further investigated the correlation between B7-H3 mRNA expression levels and LNM in EC using the RT-PCR method. Additionally, we developed and validated a diagnostic nomogram based on radiomic features for individualized preoperative prediction of LNM in patients with EC. The nomogram incorporates three components: radiomic features, B7-H3 mRNA expression levels, and LN status from CT reports.

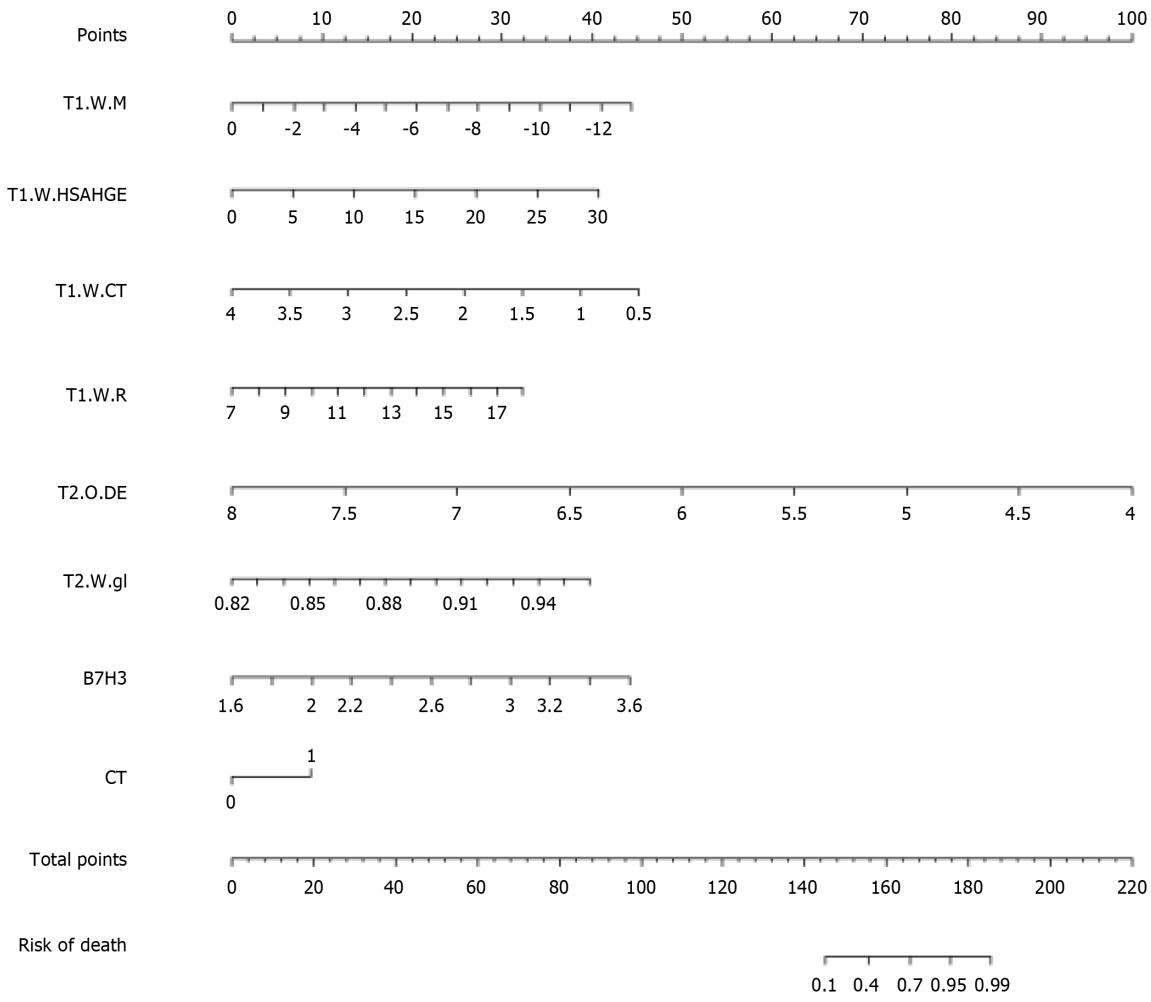

Figure 4 Developed radiomics nomogram. The radiomics nomogram was developed with the radiomics signature, B7-H3mRNA level, and computed tomography-reported lymph node status incorporated. CT: Computed tomography.

In this study, we determined the expression levels of B7-H3 mRNA in tumor tissues of EC using preoperative endoscopic biopsy. We found that the expression levels of B7-H3 mRNA were consistent with previous reports regarding LNM in EC. Additionally, our research revealed that the relative expression level of B7-H3 mRNA was significantly higher in LN-positive tissues compared to LN-negative tissues in esophageal squamous cell carcinoma. We performed ROC curve analysis and found that B7-H3 mRNA had good accuracy in predicting LNM (AUC = 0.718; 95%CI: 0.528-0.907; sensitivity: 70.3%; specificity: 70.6%). Some studies on diagnostic models have shown that relying solely on certain factors with univariate associations may not provide sufficient predictive strength[45]. However, if a factor has statistical significance, it should not be excluded from the model[46]. Therefore, in our study, we found a close association between B7-H3 and LNM, indicating the importance of B7-H3 mRNA expression in preoperative LN diagnosis.

We performed MRI image acquisition in EC patients using T2-TSE-BLADE and T1-StarVIBE sequences, which provide high image quality and anatomical details in EC and accurately depict different layers of the esophageal wall. Therefore, both T2-TSE-BLADE and T1-StarVIBE sequences are feasible for texture analysis[41]. In Python, we used the XGBoost model from the Pyradiomics package and employed leave-one-out cross-validation to extract radiomic features from the ROI in MRI. Subsequently, logistic regression analysis was conducted in R language, and based on the AIC criterion, we selected the model with the lowest entropy value. We chose six radiomic features from the extracted features, which primarily represented the tumor's texture complexity and were highly correlated with tumor heterogeneity and prognosis [47].

These extracted radiomic features, along with the B7-H3 mRNA expression and LN status from CT reports, were considered as three independent predictive factors. Subsequently, we constructed a combined prediction model using these independent risk factors. Through ROC curve analysis, our constructed combined prediction model demonstrated the highest diagnostic value in predicting LNM (AUC = 0.765; 95%CI: 0.598-0.931; sensitivity: 80.0%; specificity: 70.6%).

We applied DCA to evaluate whether the nomogram of the combined model would improve patient outcomes and thus demonstrate the clinical utility of the nomogram. DCA curves provide insights into clinical consequences based on threshold probabilities and can yield net benefits (defined as the proportion of true positives minus the proportion of false positives)[48]. Analysis of the DCA curves revealed that the combined model had higher net benefits at most threshold probabilities, suggesting that the model could be an effective approach to guide clinical decision-making and provide an accurate and reliable CDSS.

For ease of clinical application, based on the three independent risk factors from the aforementioned study, we constructed a clinical radiomic nomogram combining radiomic features, B7-H3 mRNA expression, and LN status from CT reports. This nomogram scoring system can generate the preoperative probability of LNM, enabling individualized preoperative prediction of LNM risk. Both physicians and patients can utilize the nomogram to make personalized preoperative predictions of LNM risk, aligning with the current trend of personalized medicine[49].

Certainly, this study has some limitations. Firstly, the MRI image acquisition did not include the diffusion weighted imaging (DWI) sequence, which could enrich the extracted radiomic feature library and potentially reveal more valuable radiomic features. Although DWI has demonstrated strong capabilities in distinguishing benign and malignant LN in certain cancers, the respiratory motion specific to the chest can introduce significant artifacts and affect image quality in 3.0T DWI[50]. Secondly, our study only used quantitative RT-PCR to demonstrate the mRNA expression level of B7-H3 and did not further investigate corresponding genomic features to analyze the differences between genomic and radiomic features[51]. Thirdly, although the predictive model designed in this study showed good accuracy, our sample size was relatively small, and a larger sample size would improve the confidence and performance of the LNM prediction model in EC. Fourthly, we analyzed the ROIs mainly focusing on the primary tumor and did not obtain information from the surrounding tumor-free regions, which may also contain important information. Further research is needed to address these issues.

In conclusion, a correlation was observed between B7-H3 mRNA expression levels and LNM in EC patients based on preoperative gastric endoscopic specimens. Moreover, a clinical radiomic nomogram incorporating radiomic features, B7-H3 mRNA expression levels, and LN status from CT reports was developed, enabling convenient identification of EC patients with LNM. This nomogram facilitates individualized preoperative prediction of LNM in EC patients, thereby providing guidance for the formulation of clinical treatment decisions and facilitating the selection of more rational and effective therapeutic strategies to prevent adverse patient outcomes.

CONCLUSION

This study developed a radiomics nomogram that includes radiomics features, LN status from CT reports, and B7-H3 mRNA expression, enabling convenient preoperative individualized prediction of LNM in EC patients.

ARTICLE HIGHLIGHTS

Research background

Currently, the main treatment method for esophageal cancer is surgical intervention. However, for patients with lymph node metastasis (LNM), further adjuvant chemotherapy and radiotherapy are required to support the surgical treatment. Therefore, preoperative assessment of lymph node (LN) status in esophageal cancer is of paramount importance. Currently, the preoperative diagnosis of LN status in esophageal cancer mainly relies on imaging examinations such as chest computed tomography (CT), which is limited in its diagnostic value and lacks diversity in methodology. To enhance the accurate diagnosis of preoperative LN status in esophageal cancer patients, we intend to design a clinical radiomics nomogram specifically for the diagnosis of LNM in esophageal cancer patients.

Research motivation

By developing a clinical radiomics nomogram, the preoperative LN diagnostic rate in esophageal cancer patients can be improved. This will enable a clear determination of LNM, thereby providing valuable guidance for the formulation of clinical treatment decisions. This approach aligns with the current trend in healthcare, which emphasizes the development of personalized medical treatment plans.

Research objectives

The clinical radiomics nomogram we have designed encompasses imaging radiomic features from chest magnetic resonance imaging (MRI), clinical characteristics of the patients, and the expression level of B7-H3 mRNA obtained through gastric endoscopy. All the indicators in the nomogram can be easily obtained in a clinical setting. In our study, we found that this nomogram significantly improves the diagnostic value of preoperative LN status in esophageal cancer patients compared to traditional imaging examination methods. If applied in a clinical setting in the future, it has the potential to provide valuable guidance for the formulation of clinical treatment decisions.

Research methods

In our study, we obtained esophageal cancer tissue during gastric endoscopy and used real-time quantitative polymerase chain reaction to amplify and analyze the expression level of B7-H3 mRNA. All patients underwent chest MRI examinations, and Python software packages were used to extract imaging radiomic features. Subsequently, in R language, B7-H3 mRNA, MRI radiomic features, and clinical characteristics of the patients were selected and used to construct the clinical radiomics nomogram. We further analyzed the clinical value of the nomogram using receiver operating characteristic (ROC) and decision curve analysis (DCA) curves. The results showed that the nomogram had a higher diagnostic value for preoperative LN assessment compared to traditional imaging diagnostic methods.

Research results

By quantitatively analyzing the expression of B7-H3 mRNA in 32 esophageal cancer tissues, with clinical pathological examination results as the gold standard, we plotted the ROC curve to evaluate the diagnostic value of B7-H3 for LNM in esophageal cancer. The area under the ROC curve (AUC) for B7-H3 in detecting LNM in esophageal cancer was 0.718, with a sensitivity of 73.3% and specificity of 70.6%. The optimal diagnostic threshold for B7-H3 in detecting LNM in esophageal cancer was determined to be 2.56. Using the pathological examination results as the gold standard, we calculated the LN status from CT reports, B7-H3 mRNA expression, MRI radiomic features, and a combined predictive model. Furthermore, we used ROC curves to display the diagnostic performance of CT reports, B7-H3 mRNA expression, MRI radiomic features, and the created combined predictive model for preoperative LN status. Through comparison, we found that the combined predictive model showed the best discriminative ability and predictive stability, with the highest AUC value. Based on the DCA of the combined predictive model, compared to DCA using a single radiomic feature, the addition of B7-H3 mRNA expression and clinical CT results in the combined predictive model demonstrated higher accuracy in predicting preoperative LN status. This suggests that the DCA based on this predictive model is a reliable clinical tool for predicting preoperative LN status in esophageal cancer patients. DCA indicates that the decision curve based on the combined model adds more net benefit to the "treatment" strategy when the threshold probability for patients is within the range of approximately 0.3 to 0.7.

Research conclusions

Our study has developed a clinical radiomics nomogram based on multimodal MRI, B7-H3 mRNA expression, and clinical characteristics of patients, which can be applied for preoperative LN status diagnosis in esophageal cancer patients. Compared to conventional imaging examinations, this clinical radiomics nomogram improves the accuracy of preoperative LN status diagnosis. This innovation addresses the challenge of accurately determining LN status before surgery and further facilitates optimal decision-making for the diagnosis and treatment of esophageal cancer patients. The ROC and DCA curves based on this nomogram demonstrate its significant research value in the diagnostic performance of esophageal cancer.

Research perspectives

Although the nomogram demonstrates promising diagnostic value and clinical applicability, it is important to acknowledge that the sample size in this study is relatively small. Furthermore, there was a lack of further validation cohorts to validate the nomogram. In the future, a multi-center collaborative study should be conducted to increase the sample size and design validation cohorts to confirm the effectiveness of the nomogram. Additionally, with the rapid development of genomics, integrating genomic data with radiomics may further enhance the clinical decision-making value of the designed nomogram.

FOOTNOTES

Author contributions: Xu YH performed the majority of the writing, prepared the figures and tables; Xu YH, Lu P and Gao MC performed data accusation and writing; Wang R, Li YY, Guo RQ, and Zhang WS helped proofread the abbreviations and terminology in the manuscript; Song JX provided the input in writing the paper; Xu YH and Lu P designed the outline and coordinated the writing of the paper.

Supported by The Yancheng Key Research and Development Program (Social Development), No. YCBE202324.

Institutional review board statement: The study was reviewed and approved by the Ethics Committee of Yancheng Third People's Hospital Institutional Review Board, Approval No. 2022-10.

Informed consent statement: Considering that the relevant examinations in this study do not pose significant physical or harm to the patients' interests, the requirement for obtaining informed consent from the patients has been waived by the committee.

Conflict-of-interest statement: All the authors report no relevant conflicts of interest for this article.

Data sharing statement: Technical appendix, statistical code, and dataset available from the corresponding author at jxsongycsy@163.com.

Country/Territory of origin: China

ORCID number: Yan-Han Xu 0000-0001-6230-4729; Jian-Xiang Song 0000-0003-4503-6464.

S-Editor: Li L
L-Editor: A

P-Editor: Zheng XM

REFERENCES

1 **Bray F**, Ferlay J, Soerjomataram I, Siegel RL, Torre LA, Jemal A. Global cancer statistics 2018: GLOBOCAN estimates of incidence and mortality worldwide for 36 cancers in 185 countries. *CA Cancer J Clin* 2018; **68**: 394-424 [PMID: 30207593 DOI: 10.3322/caac.21492]

2 **Chen W**, Zheng R, Baade PD, Zhang S, Zeng H, Bray F, Jemal A, Yu XQ, He J. Cancer statistics in China, 2015. *CA Cancer J Clin* 2016; **66**: 115-132 [PMID: 26808342 DOI: 10.3322/caac.21338]

3 **Smyth EC**, Lagergren J, Fitzgerald RC, Lordick F, Shah MA, Lagergren P, Cunningham D. Oesophageal cancer. *Nat Rev Dis Primers* 2017; **3**: 17048 [PMID: 28748917 DOI: 10.1038/nrdp.2017.48]

4 **Cooper JS**, Guo MD, Herskovic A, Macdonald JS, Martenson JA Jr, Al-Sarraf M, Byhardt R, Russell AH, Beitler JJ, Spencer S, Asbell SO, Graham MV, Leichman LL. Chemoradiotherapy of locally advanced esophageal cancer: long-term follow-up of a prospective randomized trial (RTOG 85-01). Radiation Therapy Oncology Group. *JAMA* 1999; **281**: 1623-1627 [PMID: 10235156 DOI: 10.1001/jama.281.17.1623]

5 **Visser E**, van Rossum PSN, Ruurda JP, van Hillegersberg R. Impact of Lymph Node Yield on Overall Survival in Patients Treated With Neoadjuvant Chemoradiotherapy Followed by Esophagectomy for Cancer: A Population-based Cohort Study in the Netherlands. *Ann Surg* 2017; **266**: 863-869 [PMID: 28742691 DOI: 10.1097/SLA.0000000000002389]

6 **Zhang HL**, Chen LQ, Liu RL, Shi YT, He M, Meng XL, Bai SX, Ping YM. The number of lymph node metastases influences survival and International Union Against Cancer tumor-node-metastasis classification for esophageal squamous cell carcinoma. *Dis Esophagus* 2010; **23**: 53-58 [PMID: 19392846 DOI: 10.1111/j.1442-2050.2009.00971.x]

7 **Rice TW**, Ishwaran H, Hofstetter WL, Schipper PH, Kesler KA, Law S, Lerut EM, Denlinger CE, Salo JA, Scott WJ, Watson TJ, Allen MS, Chen LQ, Rusch VW, Cerfolio RJ, Luketich JD, Duranceau A, Darling GE, Pera M, Apperson-Hansen C, Blackstone EH. Esophageal Cancer: Associations With (pN+) Lymph Node Metastases. *Ann Surg* 2017; **265**: 122-129 [PMID: 28009736 DOI: 10.1097/SLA.0000000000001594]

8 **Rice TW**, Lerut TE, Orringer MB, Chen LQ, Hofstetter WL, Smithers BM, Rusch VW, van Lanschot J, Chen KN, Davies AR, D'Journo XB, Kesler KA, Luketich JD, Ferguson MK, Räsänen JV, van Hillegersberg R, Fang W, Durand L, Allum WH, Cecconello I, Cerfolio RJ, Pera M, Griffin SM, Burger R, Liu JF, Allen MS, Law S, Watson TJ, Darling GE, Scott WJ, Duranceau A, Denlinger CE, Schipper PH, Ishwaran H, Apperson-Hansen C, DiPaola LM, Semple ME, Blackstone EH. Worldwide Esophageal Cancer Collaboration: neoadjuvant pathologic staging data. *Dis Esophagus* 2016; **29**: 715-723 [PMID: 27731548 DOI: 10.1111/dote.12513]

9 **Kontos F**, Michelakos T, Kurokawa T, Sadagopan A, Schwab JH, Ferrone CR, Ferrone S. B7-H3: An Attractive Target for Antibody-based Immunotherapy. *Clin Cancer Res* 2021; **27**: 1227-1235 [PMID: 33051306 DOI: 10.1158/1078-0432.CCR-20-2584]

10 **Wu CP**, Jiang JT, Tan M, Zhu YB, Ji M, Xu KF, Zhao JM, Zhang GB, Zhang XG. Relationship between co-stimulatory molecule B7-H3 expression and gastric carcinoma histology and prognosis. *World J Gastroenterol* 2006; **12**: 457-459 [PMID: 16489649 DOI: 10.3748/wjg.v12.i3.457]

11 **Loos M**, Hedderich DM, Ottenhausen M, Giese NA, Laschinger M, Esposito I, Kleeff J, Friess H. Expression of the costimulatory molecule B7-H3 is associated with prolonged survival in human pancreatic cancer. *BMC Cancer* 2009; **9**: 463 [PMID: 20035626 DOI: 10.1186/1471-2407-9-463]

12 **Bostanci O**, Sayin P, Kiziltan R, Algul S, Aydin MA, Kemik O. B7-H3: A Useful Emerging Diagnostic Marker for Colon Cancer. *Biomed Res Int* 2022; **2022**: 1523338 [PMID: 36605103 DOI: 10.1155/2022/1523338]

13 **Jin Y**, Zhang P, Li J, Zhao J, Liu C, Yang F, Yang D, Gao A, Lin W, Ma X, Sun Y. B7-H3 in combination with regulatory T cell is associated with tumor progression in primary human non-small cell lung cancer. *Int J Clin Exp Pathol* 2015; **8**: 13987-13995 [PMID: 26823710]

14 **Guery T**, Roumier C, Berthon C, Renneville A, Preudhomme C, Quesnel B. B7-H3 protein expression in acute myeloid leukemia. *Cancer Med* 2015; **4**: 1879-1883 [PMID: 26376842 DOI: 10.1002/cam4.522]

15 **Zhang T**, Jin Y, Jiang X, Li L, Qi X, Mao Y, Hua D. Clinical and Prognostic Relevance of B7-H3 and Indicators of Glucose Metabolism in Colorectal Cancer. *Front Oncol* 2020; **10**: 546110 [PMID: 33042836 DOI: 10.3389/fonc.2020.546110]

16 **Arigami T**, Narita N, Mizuno R, Nguyen L, Ye X, Chung A, Giuliano AE, Hoon DS. B7-h3 Ligand expression by primary breast cancer and associated with regional nodal metastasis. *Ann Surg* 2010; **252**: 1044-1051 [PMID: 21107115 DOI: 10.1097/SLA.0b013e3181f1939d]

17 **Chen L**, Chen J, Xu B, Wang Q, Zhou W, Zhang G, Sun J, Shi L, Pei H, Wu C, Jiang J. B7-H3 expression associates with tumor invasion and patient's poor survival in human esophageal cancer. *Am J Transl Res* 2015; **7**: 2646-2660 [PMID: 26885263]

18 **Choi J**, Kim SG, Kim JS, Jung HC, Song IS. Comparison of endoscopic ultrasonography (EUS), positron emission tomography (PET), and computed tomography (CT) in the preoperative locoregional staging of resectable esophageal cancer. *Surg Endosc* 2010; **24**: 1380-1386 [PMID: 20033712 DOI: 10.1007/s00464-009-0783-x]

19 **D'Journo XB**. Clinical implication of the innovations of the 8(th) edition of the TNM classification for esophageal and esophago-gastric cancer. *J Thorac Dis* 2018; **10**: S2671-S2681 [PMID: 30345104 DOI: 10.21037/jtd.2018.03.182]

20 **Foley K**, Findlay J, Goh V. Novel imaging techniques in staging oesophageal cancer. *Best Pract Res Clin Gastroenterol* 2018; **36-37**: 17-25 [PMID: 30551852 DOI: 10.1016/j.bpg.2018.11.009]

21 **Dappa E**, Elger T, Hasenburg A, Düber C, Battista MJ, Hötker AM. The value of advanced MRI techniques in the assessment of cervical cancer: a review. *Insights Imaging* 2017; **8**: 471-481 [PMID: 28828723 DOI: 10.1007/s13244-017-0567-0]

22 **Xu XQ**, Hu H, Su GY, Liu H, Hong XN, Shi HB, Wu FY. Utility of histogram analysis of ADC maps for differentiating orbital tumors. *Diagn Interv Radiol* 2016; **22**: 161-167 [PMID: 26829400 DOI: 10.5152/dir.2015.15202]

23 **Qu J**, Zhang H, Wang Z, Zhang F, Liu H, Ding Z, Li Y, Ma J, Zhang Z, Zhang S, Dong Y, Jiang L, Zhang W, Grimm R, Kiefer B, Kamel IR, Qin J, Li H. Comparison between free-breathing radial VIBE on 3-T MRI and endoscopic ultrasound for preoperative T staging of resectable oesophageal cancer, with histopathological correlation. *Eur Radiol* 2018; **28**: 780-787 [PMID: 28799124 DOI: 10.1007/s00330-017-4963-0]

24 **Xu YH**, Lu P, Gao MC, Wang R, Li YY, Song JX. Progress of magnetic resonance imaging radiomics in preoperative lymph node diagnosis of esophageal cancer. *World J Radiol* 2023; **15**: 216-225 [PMID: 37545645 DOI: 10.4329/wjr.v15.i7.216]

25 **Xie C**, Hu Y, Han L, Fu J, Vardhanabhuti V, Yang H. Prediction of Individual Lymph Node Metastatic Status in Esophageal Squamous Cell Carcinoma Using Routine Computed Tomography Imaging: Comparison of Size-Based Measurements and Radiomics-Based Models. *Ann Surg Oncol* 2022; **29**: 8117-8126 [PMID: 36018524 DOI: 10.1245/s10434-022-12207-7]

26 **Lambin P**, Rios-Velazquez E, Leijenaar R, Carvalho S, van Stiphout RG, Granton P, Zegers CM, Gillies R, Boellard R, Dekker A, Aerts HJ. Radiomics: extracting more information from medical images using advanced feature analysis. *Eur J Cancer* 2012; **48**: 441-446 [PMID: 22257792 DOI: 10.1016/j.ejca.2011.11.036]

27 **Lambin P**, Leijenaar RTH, Deist TM, Peerlings J, de Jong EEC, van Timmeren J, Sanduleanu S, Larue RTHM, Even AJG, Jochems A, van Wijk Y, Woodruff H, van Soest J, Lustberg T, Roelofs E, van Elmpt W, Dekker A, Mottaghy FM, Wildberger JE, Walsh S. Radiomics: the bridge between medical imaging and personalized medicine. *Nat Rev Clin Oncol* 2017; **14**: 749-762 [PMID: 28975929 DOI: 10.1038/nrclinonc.2017.141]

28 **Liu C**, Ding J, Spuhler K, Gao Y, Serrano Sosa M, Moriarty M, Hussain S, He X, Liang C, Huang C. Preoperative prediction of sentinel lymph node metastasis in breast cancer by radiomic signatures from dynamic contrast-enhanced MRI. *J Magn Reson Imaging* 2019; **49**: 131-140 [PMID: 30171822 DOI: 10.1002/jmri.26224]

29 **Huang YQ**, Liang CH, He L, Tian J, Liang CS, Chen X, Ma ZL, Liu ZY. Development and Validation of a Radiomics Nomogram for Preoperative Prediction of Lymph Node Metastasis in Colorectal Cancer. *J Clin Oncol* 2016; **34**: 2157-2164 [PMID: 27138577 DOI: 10.1200/JCO.2015.65.9128]

30 **Coroller TP**, Agrawal V, Huynh E, Narayan V, Lee SW, Mak RH, Aerts HJWL. Radiomic-Based Pathological Response Prediction from Primary Tumors and Lymph Nodes in NSCLC. *J Thorac Oncol* 2017; **12**: 467-476 [PMID: 27903462 DOI: 10.1016/j.jtho.2016.11.2226]

31 **Gabriel E**, Attwood K, Du W, Tuttle R, Alnaji RM, Nurkin S, Malhotra U, Hochwald SN, Kukar M. Association Between Clinically Staged Node-Negative Esophageal Adenocarcinoma and Overall Survival Benefit From Neoadjuvant Chemoradiation. *JAMA Surg* 2016; **151**: 234-245 [PMID: 26559488 DOI: 10.1001/jamasurg.2015.4068]

32 **Sugawara K**, Yamashita H, Uemura Y, Mitsui T, Yagi K, Nishida M, Aikou S, Mori K, Nomura S, Seto Y. Numeric pathologic lymph node classification shows prognostic superiority to topographic pN classification in esophageal squamous cell carcinoma. *Surgery* 2017; **162**: 846-856 [PMID: 28739092 DOI: 10.1016/j.surg.2017.06.013]

33 **Campbell NP**, Villaflor VM. Neoadjuvant treatment of esophageal cancer. *World J Gastroenterol* 2010; **16**: 3793-3803 [PMID: 20698042 DOI: 10.3748/wjg.v16.i30.3793]

34 **Mayerhoefer ME**, Materka A, Langs G, Häggström I, Szczypiński P, Gibbs P, Cook G. Introduction to Radiomics. *J Nucl Med* 2020; **61**: 488-495 [PMID: 32060219 DOI: 10.2967/jnumed.118.222893]

35 **Bera K**, Braman N, Gupta A, Velcheti V, Madabhushi A. Predicting cancer outcomes with radiomics and artificial intelligence in radiology. *Nat Rev Clin Oncol* 2022; **19**: 132-146 [PMID: 34663898 DOI: 10.1038/s41571-021-00560-7]

36 **Conti A**, Duggento A, Indovina I, Guerrisi M, Toschi N. Radiomics in breast cancer classification and prediction. *Semin Cancer Biol* 2021; **72**: 238-250 [PMID: 32371013 DOI: 10.1016/j.semcancer.2020.04.002]

37 **Han L**, Zhu Y, Liu Z, Yu T, He C, Jiang W, Kan Y, Dong D, Tian J, Luo Y. Radiomic nomogram for prediction of axillary lymph node metastasis in breast cancer. *Eur Radiol* 2019; **29**: 3820-3829 [PMID: 30701328 DOI: 10.1007/s00330-018-5981-2]

38 **Liu J**, Sun D, Chen L, Fang Z, Song W, Guo D, Ni T, Liu C, Feng L, Xia Y, Zhang X, Li C. Radiomics Analysis of Dynamic Contrast-Enhanced Magnetic Resonance Imaging for the Prediction of Sentinel Lymph Node Metastasis in Breast Cancer. *Front Oncol* 2019; **9**: 980 [PMID: 31632912 DOI: 10.3389/fonc.2019.00980]

39 **Qiu Q**, Duan J, Deng H, Han Z, Gu J, Yue NJ, Yin Y. Development and Validation of a Radiomics Nomogram Model for Predicting Postoperative Recurrence in Patients With Esophageal Squamous Cell Cancer Who Achieved pCR After Neoadjuvant Chemoradiotherapy Followed by Surgery. *Front Oncol* 2020; **10**: 1398 [PMID: 32850451 DOI: 10.3389/fonc.2020.01398]

40 **Yu Y**, Tan Y, Xie C, Hu Q, Ouyang J, Chen Y, Gu Y, Li A, Lu N, He Z, Yang Y, Chen K, Ma J, Li C, Ma M, Li X, Zhang R, Zhong H, Ou Q, Zhang Y, He Y, Li G, Wu Z, Su F, Song E, Yao H. Development and Validation of a Preoperative Magnetic Resonance Imaging Radiomics-Based Signature to Predict Axillary Lymph Node Metastasis and Disease-Free Survival in Patients With Early-Stage Breast Cancer. *JAMA Netw Open* 2020; **3**: e2028086 [PMID: 33289845 DOI: 10.1001/jamanetworkopen.2020.28086]

41 **Qu J**, Shen C, Qin J, Wang Z, Liu Z, Guo J, Zhang H, Gao P, Bei T, Wang Y, Liu H, Kamel IR, Tian J, Li H. The MR radiomic signature can predict preoperative lymph node metastasis in patients with esophageal cancer. *Eur Radiol* 2019; **29**: 906-914 [PMID: 30039220 DOI: 10.1007/s00330-018-5583-z]

42 **Shen C**, Liu Z, Wang Z, Guo J, Zhang H, Wang Y, Qin J, Li H, Fang M, Tang Z, Li Y, Qu J, Tian J. Building CT Radiomics Based Nomogram for Preoperative Esophageal Cancer Patients Lymph Node Metastasis Prediction. *Transl Oncol* 2018; **11**: 815-824 [PMID: 29727831 DOI: 10.1016/j.tranon.2018.04.005]

43 **Toiyama Y**, Inoue Y, Shimura T, Fujikawa H, Saigusa S, Hiro J, Kobayashi M, Ohi M, Araki T, Tanaka K, Mohri Y, Kusunoki M. Serum Angiopoietin-like Protein 2 Improves Preoperative Detection of Lymph Node Metastasis in Colorectal Cancer. *Anticancer Res* 2015; **35**: 2849-2856 [PMID: 25964566]

44 **Birkhahn M**, Mitra AP, Cote RJ. Molecular markers for bladder cancer: the road to a multimarker approach. *Expert Rev Anticancer Ther* 2007; **7**: 1717-1727 [PMID: 18062746 DOI: 10.1586/14737140.7.12.1717]

45 **Yu SC**, Qi X, Hu YH, Zheng WJ, Wang QQ, Yao HY. [Overview of multivariate regression model analysis and application]. *Zhonghua Yu Fang Yi Xue Za Zhi* 2019; **53**: 334-336 [PMID: 30841679 DOI: 10.3760/cma.j.issn.0253-9624.2019.03.020]

46 **Collins GS**, Reitsma JB, Altman DG, Moons KG. Transparent reporting of a multivariable prediction model for individual prognosis or diagnosis (TRIPOD): the TRIPOD statement. *BMJ* 2015; **350**: g7594 [PMID: 25569120 DOI: 10.1136/bmj.g7594]

47 **Yip C**, Davnall F, Kozarski R, Landau DB, Cook GJ, Ross P, Mason R, Goh V. Assessment of changes in tumor heterogeneity following neoadjuvant chemotherapy in primary esophageal cancer. *Dis Esophagus* 2015; **28**: 172-179 [PMID: 24460831 DOI: 10.1111/dote.12170]

48 **Van Calster B**, Wynants L, Verbeek JFM, Verbakel JY, Christodoulou E, Vickers AJ, Roobol MJ, Steyerberg EW. Reporting and Interpreting Decision Curve Analysis: A Guide for Investigators. *Eur Urol* 2018; **74**: 796-804 [PMID: 30241973 DOI: 10.1016/j.eururo.2018.08.038]

49 **Balachandran VP**, Gonen M, Smith JJ, DeMatteo RP. Nomograms in oncology: more than meets the eye. *Lancet Oncol* 2015; **16**: e173-e180 [PMID: 25846097 DOI: 10.1016/S1470-2045(14)71116-7]

50 **Holzapfel K**, Gaa J, Schubert EC, Eiber M, Kleeff J, Rummeny EJ, Loos M. Value of diffusion-weighted MR imaging in the diagnosis of lymph node metastases in patients with cholangiocarcinoma. *Abdom Radiol (NY)* 2016; **41**: 1937-1941 [PMID: 27271285 DOI: 10.1007/s00261-016-0791-y]

51 **Nakarai C**, Osawa K, Akiyama M, Matsubara N, Ikeuchi H, Yamano T, Hirota S, Tomita N, Usami M, Kido Y. Expression of AKR1C3 and CNN3 as markers for detection of lymph node metastases in colorectal cancer. *Clin Exp Med* 2015; **15**: 333-341 [PMID: 24934327 DOI: 10.1007/s10238-014-0298-1]

Published by **Baishideng Publishing Group Inc**
7041 Koll Center Parkway, Suite 160, Pleasanton, CA 94566, USA
Telephone: +1-925-3991568
E-mail: office@baishideng.com
Help Desk: https://www.f6publishing.com/helpdesk
https://www.wjgnet.com